

# The sensitivity of seafloor compliance to two-dimensional low-velocity anomalies

Tom Hulme, Wayne C. Crawford and S. C. Singh

*Institut de Physique du Globe de Paris, 4 place Jussieu, 75005 Paris, France. E-mail: crawford@ipgp.jussieu.fr*

Accepted 2005 July 19. Received 2005 April 27; in original form 2004 June 9

## SUMMARY

Seafloor compliance (the deformation of the seafloor under pressure forcing by long wavelength ocean surface waves) is a passive source geophysical measurement that is particularly sensitive to subsurface *S*-wave velocity. Existing inversions of seafloor compliance data for *S*-wave structure assume a 1-D velocity model, whereas in reality there may be significant lateral velocity variation. The effect of 2-D structure on compliance measurements has previously been investigated using finite differences, but computational constraints limit the number and type of models that can be tested. We present a quasi-analytical calculation of seafloor compliance over a cylinder that allows us to efficiently investigate the effect of an important subset of subsurface models, including pure fluid inclusions. The compliance displays the same sensitivity to regions of low shear modulus as is seen for 1-D situations, generating a strong peak over the low-velocity zone. The spatial width of this peak, which is a measure of the horizontal resolution of seafloor compliance, is approximately proportional to the depth of the cylinder, while its amplitude is controlled by the radius and depth of the cylinder and the *S*-wave speed of the cylinder and the background. Minimum structure 1-D inversions of the compliance measured above a fluid cylinder recover distinct low-velocity zones, although the recovered *S*-wave speed is much greater than zero, and the low-velocity zone is smeared out over a greater depth range than that occupied by the cylinder.

**Key words:** low-velocity zone, melt, scattering, shear modulus, *S*-waves.

## 1 INTRODUCTION

Seafloor compliance is a measure of seafloor deformation under pressure forcing by long wavelength ocean surface waves. Compliance is measured using a broadband seismometer (OBS) and a low-frequency pressure gauge deployed autonomously on the seafloor; the compliance measurement is obtained in the frequency domain as the ratio of the vertical component of seafloor motion to the applied pressure (Crawford *et al.* 1991). Seafloor compliance is inversely proportional to the subsurface shear modulus, making compliance measurements particularly sensitive to the presence of fluids in the crust. The ocean waves that generate the compliance signal span a range of wavelengths, with each wavelength sensitive to structure at a different depth.

Forward calculations of seafloor compliance for laterally uniform velocity structures can easily be made using a propagator matrix method (Crawford *et al.* 1991), and illustrate the particular sensitivity of the technique to regions of low *S*-wave velocity. Fig. 1 shows a simple example, for the case of a low-velocity layer embedded in a uniform background. The low-velocity zone is responsible for the peak in the compliance function; the frequency at which this maximum occurs is a function of the layer's depth. It is also straightforward to perform 1-D inversion of compliance data to determine

subsurface *S*-wave structure. Synthetic tests have demonstrated the ability of this type of approach to successfully recover complex *S*-wave structures (Crawford 2004).

The 1-D assumption is clearly a gross simplification, however, and it is important to understand the effect of lateral variations in structure. Indeed, extensive compliance measurements from 9–10°N on the East Pacific Rise show significant across-axis variation, and (1-D) inversions of the data produce different velocity structures on and off-axis (Crawford & Webb 2002). At 9°48'N, for example, minimum structure inversions of on-axis data find low-velocity zones at both shallow (1.5 km) and Moho depths, whereas no such zones are found in inversions of data recorded 4.7 km and 7.6 km off-axis. To understand the effect of this lateral variation on the reliability of 1-D inversions, we must investigate the sensitivity of seafloor compliance to variations in 2-D structure.

The problem of calculating compliance for 2-D structure was firstly considered by Crawford *et al.* (1998), using a finite-difference modelling technique. This study showed that the qualitative behaviour of compliance for 2-D models was the same as that for 1-D models, exhibiting the characteristic sensitivity to the presence of regions of low *S*-wave velocity. Finite-difference calculations face severe limitations, however, because of their large computational cost and poor lateral resolution. The wavelength of

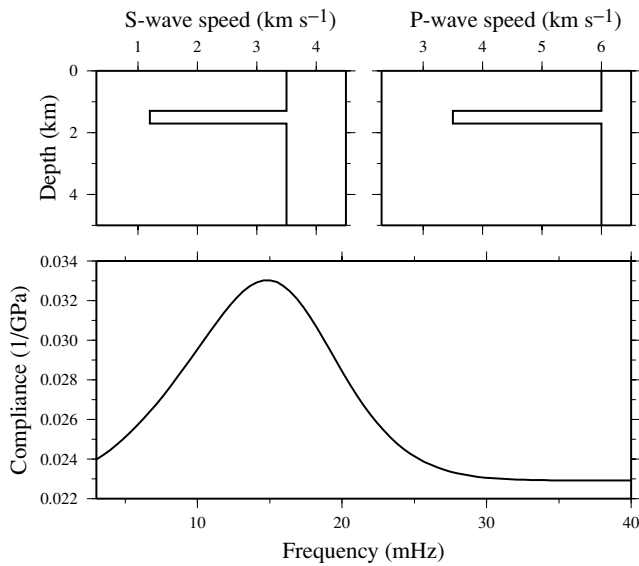


**Figure 1.** An example of a 1-D seafloor compliance calculation for a 400 m thick low-velocity layer (of  $P$ -wave speed  $3.5 \text{ km s}^{-1}$ ,  $S$ -wave speed  $1.2 \text{ km s}^{-1}$  and density  $2700 \text{ kg m}^{-3}$ ) embedded in a uniform background (of  $P$ -wave speed  $6 \text{ km s}^{-1}$ ,  $S$ -wave speed  $3.5 \text{ km s}^{-1}$  and density  $2700 \text{ kg m}^{-3}$ ). The compliance shows a peak caused by the presence of the layer. The water depth is 2.7 km.

the forcing that generates the compliance signal is on the order of 2–40 km, which consequently forces the computational domain to be very large in comparison to typical features of interest. Furthermore, Crawford *et al.* (1998) found it necessary to smooth out variations in the material properties of their models over a range of 1.2–1.5 km, making it difficult to calculate compliance over small crustal features. Recently, a 3-D finite-difference model has been developed to study the effect of gas hydrates on the seafloor compliance response (Latychev & Edwards 2003). However, these finite-difference algorithms remain too computationally intensive for comprehensive sensitivity studies, where we require the ability to run a large number of models in a short space of time.

In this paper we investigate more fully the sensitivity of compliance to 2-D structure. To limit the number of parameters in the problem, and to allow the use of an efficient modelling scheme, we consider only the simple case of a cylindrical object embedded in a uniform background. The key to this effort is a quasi-analytical solution of the compliance over a cylinder that we present in this paper. The method, based on a partial wave expansion of the incident and scattered wave potentials, has previously been used to study the scattering of elastic waves by cylindrical targets (Liu *et al.* 2000), but has never before been applied to the compliance problem.

This method calculates the compliance over a cylinder accurately and efficiently (around 1000 times faster than a finite-difference simulation would be). We are thus able to run a comprehensive range of models to investigate the effect of a discrete body on seafloor compliance. Furthermore, we are able to model directly the compliance over a pure fluid inclusion, whereas finite-difference methods become unstable if very low  $S$ -wave velocities are used in the model. Isolated melt bodies may play an important role in the generation of oceanic crust at mid ocean ridges (Kelemen & Aharonov 1998; Maclennan *et al.* 2005), and more generally, isolated fluid bodies represent an end-member case for seafloor com-

pliance: in the 1-D case, a pure fluid body creates a delta function in compliance.

The method as implemented is limited to cylinders, but the simplicity of these models allows us to fully characterize the effect of the size, depth and  $S$ -wave velocity of these intrusions on compliance. We use this tool to comprehensively explore the variations in compliance for a large range of models, including regions of parameter space that cannot be reached using finite-difference methods. 1-D inversions of our synthetic calculations then allow us to see how well the true velocity structure is recovered, providing insight into the suitability and shortcomings of this approximation technique for settings where lateral variation is important.

## 2 THEORY: COMPLIANCE OF A CYLINDER

The geometry of the model problem is shown in Fig. 2. We can calculate the compliance over a cylindrical object using an extension of the classical result for the  $P$ - $SV$  scattering of a propagating plane wave by an elastic cylinder (e.g. Pao & Mow 1973). This solution is based on a partial wave expansion of the incident and scattered wave potentials for the wavefield in the background: in Cartesian coordinates we write the wavefield as

$$u_x = \frac{\partial \phi}{\partial x} + \frac{\partial \psi}{\partial z}, \quad u_z = \frac{\partial \phi}{\partial z} - \frac{\partial \psi}{\partial x}, \quad (1)$$

while in angular coordinates the decomposition becomes

$$u_r = \frac{\partial \phi}{\partial r} + \frac{1}{r} \frac{\partial \psi}{\partial \theta}, \quad u_\theta = \frac{1}{r} \frac{\partial \phi}{\partial \theta} - \frac{\partial \psi}{\partial r}. \quad (2)$$

The  $P$ - and  $S$ -wave potentials  $\phi$  and  $\psi$  for waves of angular frequency  $\omega$  satisfy the Helmholtz equations

$$\left( \nabla^2 + \frac{\omega^2}{\alpha^2} \right) \phi = 0, \quad (3)$$

$$\left( \nabla^2 + \frac{\omega^2}{\beta^2} \right) \psi = 0, \quad (4)$$

where  $\alpha$  and  $\beta$  are the  $P$ - and  $S$ -wave speeds of the background. As is well-known, separating the Helmholtz equation in cylindrical coordinates gives solutions that can be written in terms of Bessel functions  $J_m(r)$  and  $Y_m(r)$ . For an incident plane  $P$  wave travelling

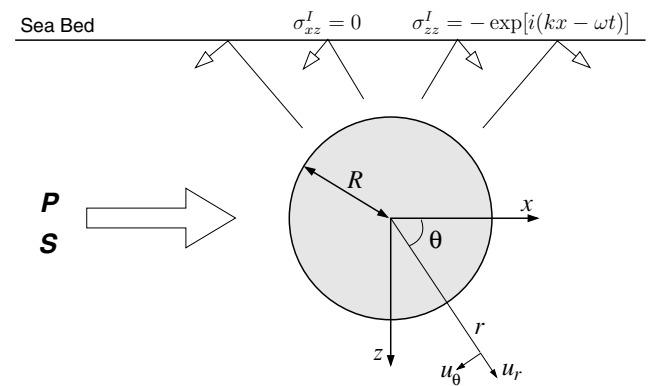


**Figure 2.** The geometry of the cylinder scattering problem. An incident wavefield of  $P$  and  $S$  waves, satisfying the conditions  $\sigma_{xz}^I = 0$ ,  $\sigma_{zz}^I = -e^{i(kx - \omega t)}$  at the seabed, is incident on a cylindrical heterogeneity of radius  $R$ . The scattered displacement field is evaluated at the seabed and can be used to calculate the compliance.

in the  $x$ -direction we have the explicit representation of the incident potential

$$\phi^I = \exp \left[ i\omega \left( \frac{x}{\alpha} - t \right) \right] \quad (5)$$

$$= \exp \left[ i\omega \left( \frac{r}{\alpha} \cos \theta - t \right) \right] \quad (6)$$

$$= e^{-i\omega t} \sum_{m=0}^{\infty} \epsilon_m i^m J_m(\omega r / \alpha) \cos(m\theta), \quad (7)$$

where  $\epsilon_m$  is the Neumann factor defined by  $\epsilon_0 = 1$  and  $\epsilon_m = 2$  if  $m > 0$  (e.g. Jeffreys & Jeffreys 1956). The potentials for the scattered waves are most easily written in terms of the Hankel function of the first kind,  $H_m^{(1)}(r) = J_m(r) + iY_m(r)$ , as

$$\phi_P^S = e^{-i\omega t} \sum_{m=0}^{\infty} A_m H_m^{(1)}(\omega r / \alpha) \cos(m\theta), \quad (8)$$

$$\psi_P^S = e^{-i\omega t} \sum_{m=1}^{\infty} B_m H_m^{(1)}(\omega r / \beta) \sin(m\theta). \quad (9)$$

Similarly, an incident plane  $SV$  wave has potential

$$\psi^I = e^{-i\omega t} \sum_{m=0}^{\infty} \epsilon_m i^m J_m(\omega r / \beta) \cos(m\theta), \quad (10)$$

and generates scattered  $P$  and  $SV$  waves with potentials

$$\phi_S^S = e^{-i\omega t} \sum_{m=1}^{\infty} C_m H_m^{(1)}(\omega r / \alpha) \sin(m\theta), \quad (11)$$

$$\psi_S^S = e^{-i\omega t} \sum_{m=0}^{\infty} D_m H_m^{(1)}(\omega r / \beta) \cos(m\theta). \quad (12)$$

The wavefield within the cylinder can be represented by analogous expressions, although these will not concern us here. Algebraic expressions for the coefficients  $A_m$ ,  $B_m$ ,  $C_m$  and  $D_m$  (in terms of the material properties of the cylinder and the background, the frequency and wavenumber of the wave and the size of the cylinder) are given by Liu *et al.* (2000), although they could equally well be calculated purely numerically by imposing the boundary conditions that displacement and traction are continuous at the cylinder's surface. Different expressions are used according to whether the cylinder is fluid or elastic.

To apply this solution to the problem of compliance, we extend it to calculate the scattering from an incident evanescent wave. An evanescent wave has a potential of the form  $\exp(ik_x x - k_z z - i\omega t)$ , where the horizontal wavenumber  $k_x$  and the vertical wavenumber  $k_z$  are related by

$$k_z^2 = k_x^2 - \frac{\omega^2}{c^2}, \quad c = \alpha, \beta. \quad (13)$$

An analytic continuation of the representation (5)–(12) to  $\theta \in \mathbb{C}$ , together with the substitution

$$\theta \rightarrow \theta - i \tanh^{-1} \left( \frac{k_z}{k_x} \right) \quad (14)$$

allows the same algebraic expressions for  $A_m$ ,  $B_m$ ,  $C_m$  and  $D_m$  to be used in calculating scattering from evanescent waves as from propagating waves.

We consider a combination of evanescent incident  $P$  and  $SV$  waves chosen to satisfy the conditions  $\sigma_{xz}^I = 0$ ,  $\sigma_{zz}^I = -e^{i(kx - \omega t)}$  at the

seabed, with  $\omega$  and  $k$  satisfying the gravity wave dispersion relationship (e.g. Acheson 1990)

$$\omega^2 = gk \tanh kH, \quad (15)$$

where  $g$  is the acceleration due to gravity and  $H$  is the water depth. These incident waves generate a scattered wavefield, the upgoing part of which is reflected at the seabed, which acts as a free surface. We calculate the scattered displacement field  $u_z^S$  at the seabed taking into account the free surface reflection, and since we also know the incident wavefield  $u_z^I$  it is straightforward to calculate the compliance as

$$\xi = k \frac{u_z^S + u_z^I}{\sigma_{zz}^I}. \quad (16)$$

We make the Born assumption that the scattered wavefield is much smaller than the incident wavefield, and so neglect any multiple scattering between the seabed and the cylinder. The validity of this assumption can be checked *a posteriori* by comparing the size of the incident and scattered wavefields.

### 3 COMPLIANCE CALCULATIONS

#### 3.1 Example

An example of the results of a compliance calculation is shown in Fig. 3. This particular case is for a low-velocity cylinder of radius 600 m placed with centre at a depth 1.5 km below the seabed. The cylinder has a  $P$ -wave speed of 3.5 km s<sup>-1</sup> and an  $S$ -wave speed of 1.2 km s<sup>-1</sup>, while the background has a  $P$ -wave speed of 6 km s<sup>-1</sup> and an  $S$ -wave speed of 3.5 km s<sup>-1</sup>. Both background and cylinder have a density of 2700 kg m<sup>-3</sup>, and the water depth is 2.7 km. These wave speeds are the same as for the 1-D example of Fig. 1, and are comparable to the situation for a low-velocity mush zone that might be found beneath the East Pacific Rise (e.g. Singh *et al.* 1998).

The compliance function is dominated by a strong peak centred over the anomaly, sharply localized in space and broadly localized in frequency. The highest amplitudes are found directly over the centre of the cylinder; at large distances offset from the centre of the cylinder and at high frequencies the function decays to the compliance of the background. A graph of the compliance at zero offset as a function of frequency (Fig. 3b) shows a similar shape to the 1-D calculation of Fig. 1. However, in the 2-D case, the amplitudes of the response are smaller, the peak is wider in frequency, and the maximum compliance occurs at a higher frequency. At larger offsets the compliance peak shifts to lower frequencies. These observations are in agreement with the finite-difference calculations of Crawford *et al.* (1998). The spatial localization of the compliance function is evident from plots of compliance as a function of position at various fixed frequencies (Fig. 3c). At a frequency of 17.5 mHz (approximately the frequency at which the peak compliance is found), the compliance decays over a spatial half-width of around 2.5 km away from the centre of the cylinder. The low-amplitude ripples that are found at larger offsets are a manifestation of the Rayleigh wave that is generated when the scattering from the cylinder reflects at the seabed.

#### 3.2 Sensitivity tests

The general nature of the compliance function for this particular example—a peak centred over the cylinder, localized in space and frequency—is very typical of the response as various parameters

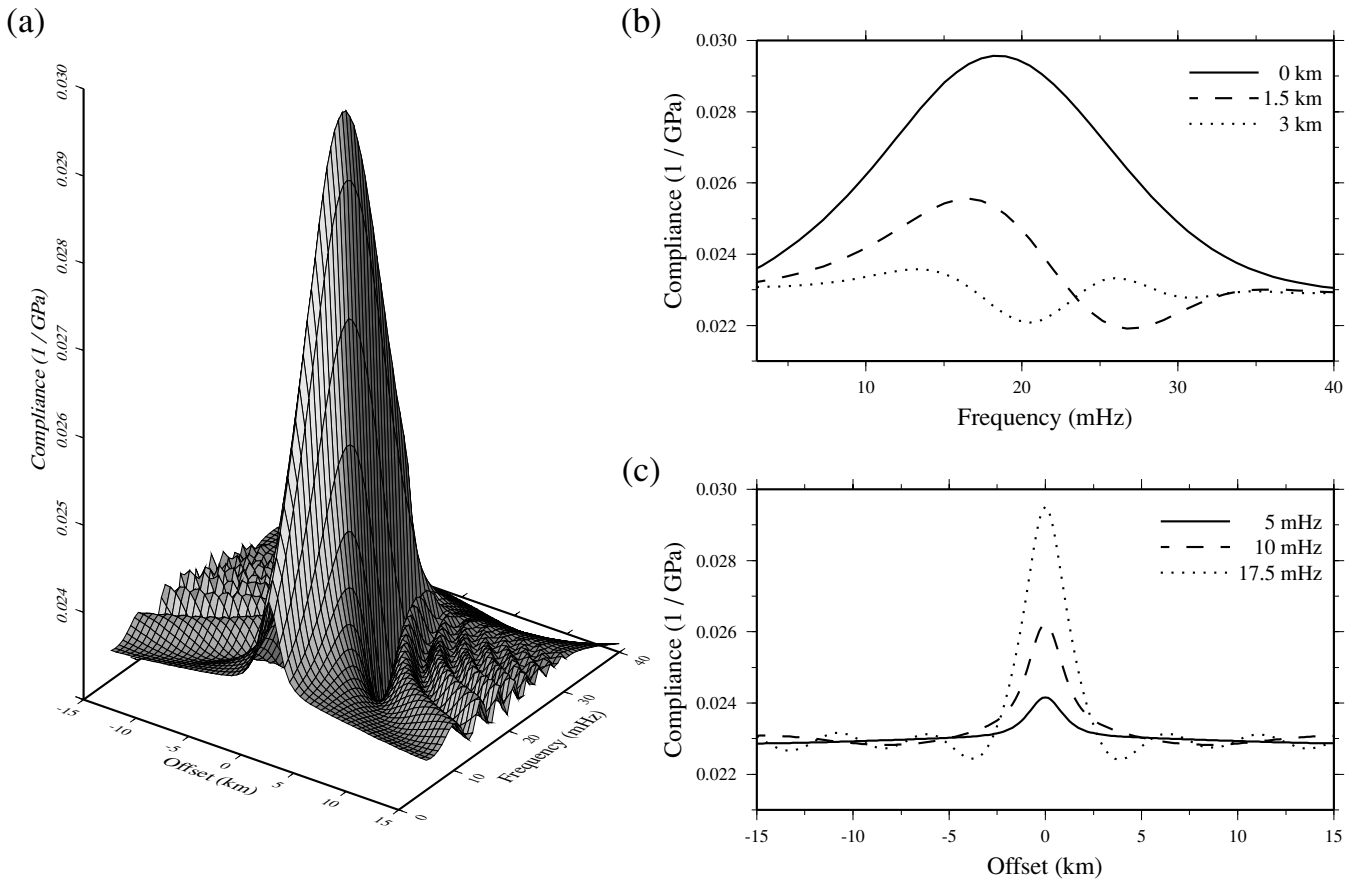


**Figure 3.** The amplitude of the compliance over a 600 m radius mush cylinder placed at a depth of 1.5 km. (a) Compliance as a function of both frequency and offset. (b) Compliance as a function of frequency at selected offsets. (c) Compliance as a function of offset at selected frequencies.

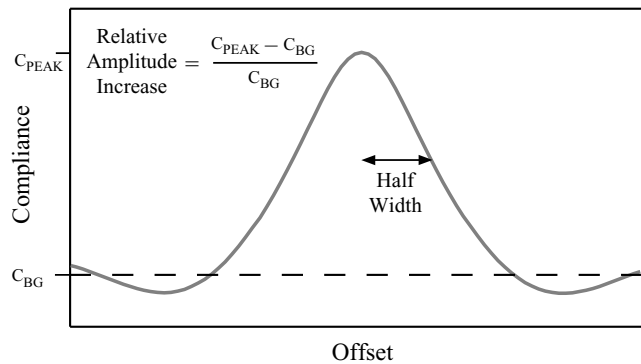


**Figure 4.** Definitions of half-width and relative amplitude increase. The maximum compliance (measured directly over the centre of the cylinder) is  $C_{PEAK}$ , while the compliance of a half-space with material properties equal to those of the background is  $C_{BG}$ . The relative amplitude increase is given by  $(C_{PEAK} - C_{BG})/C_{BG}$ , while the half-width is defined by the offset at which the compliance measurement drops to halfway between  $C_{PEAK}$  and  $C_{BG}$ .

of the problem are changed. To a first approximation, we can characterize the compliance function by three measurements (Fig. 4):

- (i) the amplitude of the peak relative to the compliance of the background;
- (ii) the frequency at which this peak occurs (or equivalently the corresponding wavelength of the forcing gravity wave) and
- (iii) the half-width of the spatial decay of the peak, measured at the peak frequency.

Running a range of models allows us to investigate the sensitivity of these measures to the parameters of the model: the radius and depth of the cylinder and the material properties of the cylinder and the background. We do not aim to produce a complete characterization of the compliance response for all possible cylinders, but instead to focus on examples of geophysical relevance. To this end, our sensitivity tests are based around three models, each of which represents a situation that may be found under a mid-ocean ridge. The first model, a medium-sized mush cylinder at shallow depth, was introduced in the example calculation of the previous section. The second model is of a small pure fluid cylinder at shallow depth, and the third model is a large mush cylinder at Moho depth.

The small shallow fluid cylinder has a radius of 300 m and is placed with centre at a depth of 1.5 km. It has a  $P$ -wave speed of  $3 \text{ km s}^{-1}$  and an  $S$ -wave speed of zero. As before, the background has a  $P$ -wave speed of  $6 \text{ km s}^{-1}$  and an  $S$ -wave speed of  $3.5 \text{ km s}^{-1}$ . Both cylinder and background have a density of  $2700 \text{ kg m}^{-3}$  and the water depth is 2.7 km. The compliance response for this model is shown in Fig. 5. Compared to the results for the medium shallow mush cylinder shown in Fig. 3, the amplitude of the compliance response is smaller, while the frequency of the peak response and the spatial half-width of the peak are about the same for the two models.

The large deep mush cylinder has a radius of 1200 m with centre at a depth of 5 km. It has a  $P$ -wave speed of  $3.5 \text{ km s}^{-1}$  and an  $S$ -wave speed of  $1.2 \text{ km s}^{-1}$ . All other details are as before. The compliance response plotted in Fig. 6 shows a peak that is comparable in amplitude to the small fluid cylinder, but centred at a lower

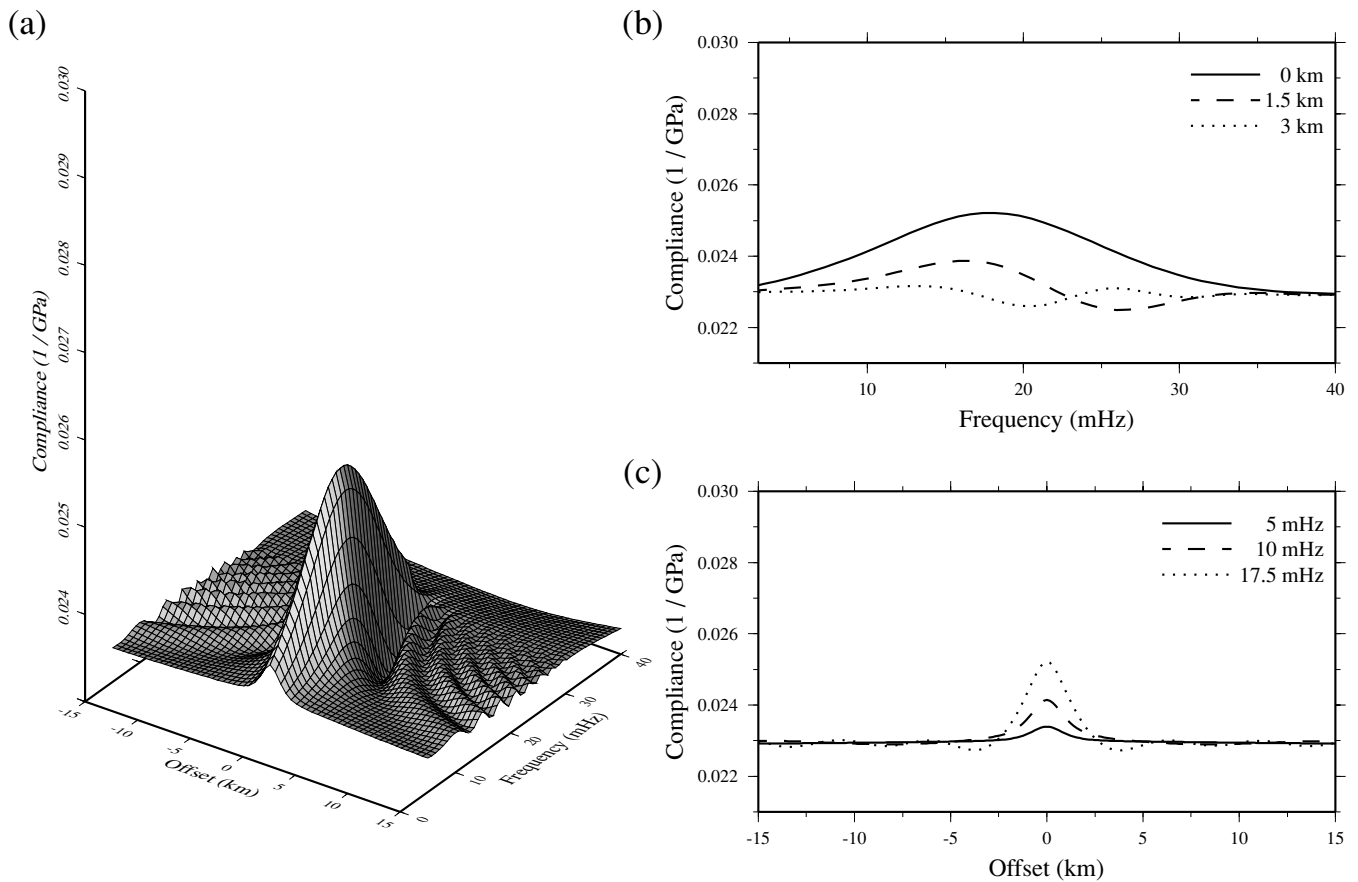


**Figure 5.** The amplitude of the compliance over a 300 m radius fluid cylinder placed at a depth of 1.5 km. (a) Compliance as a function of both frequency and offset. (b) Compliance as a function of frequency at selected offsets. (c) Compliance as a function of offset at selected frequencies.

frequency. The spatial half-width (about 8 km) is larger than that for the peaks generated by the shallow cylinders, and the compliance decays more quickly with increasing frequency. It is noticeable that the compliance peak for this model is restricted to a narrower range of frequencies than for the cylinders at shallow depth. Crawford & Webb (2002) interpret narrowband peaks in compliance measurements from  $9^{\circ}48'$  on the East Pacific Rise as being indicative of Moho-level melt bodies, and this is supported by the 2-D modelling here. Although these deep low-velocity zones may have large spatial half-widths, they affect the compliance over a narrow range of frequencies.

For each of these three models we carry out systematic sensitivity tests, varying one parameter of the model while keeping all others fixed. In this way we are able to characterize the compliance of a large number of models (over 400 different models were used to produce the sensitivity figures below). Just as in the 1-D case, it is found that compliance is virtually insensitive to changes in density and  $P$ -wave speed. The results presented below therefore only consider changes to the  $S$ -wave speed, cylinder depth and cylinder radius of the models.

### 3.2.1 Sensitivity to $S$ -wave speed

We are able to vary the  $S$ -wave speed of both the background and cylinder for each of our models, and the results of these sensitivity tests are shown in Fig. 7. Each symbol plotted on the graphs corresponds to a different model: circles to the small shallow fluid cylinder, triangles to the medium shallow mush cylinder and squares

to the large deep mush cylinder. The solid black symbols mark the points on the graph where the parameter that is being varied passes through the value used in the original model. Whenever we change an  $S$ -wave speed we have the choice of either keeping the corresponding  $P$ -wave fixed (and thus allowing the Poisson ratio to vary) or to fix the Poisson ratio and allow the  $P$ -wave speed to vary along with the  $S$ -wave speed. The solid light grey symbols correspond to changes in the  $S$ -wave speed with the Poisson ratio fixed, while the hollow symbols are the case when the  $P$ -wave speed is fixed. The results of the sensitivity tests are very similar in the two cases, illustrating the relative insensitivity of the compliance response to the  $P$ -wave speed.

The primary effect on changing the  $S$ -wave speed of the cylinder is on the relative amplitude increase of the compliance peak. As  $S$ -wave speed of the cylinder is reduced, the relative amplitude increase of the compliance anomaly gets larger, although the size of this increase tails off as the wave speed tends to zero. The sensitivity to changes in  $S$ -wave speed of the cylinder is, therefore, greatest at non-zero values of the wave speed. This pattern of behaviour is in marked contrast to 1-D behaviour, where the sensitivity to changes in  $S$ -wave speed is greatest at low values of the wave speed (Crawford *et al.* 1991).

In the case of the small shallow fluid cylinder, as we move the  $S$ -wave speed to non-zero values, the cylinder is no longer fluid and the full elastic solution must be used (it is also clearly not possible to change the wave speed to a non-zero value and keep the Poisson ratio fixed). The sensitivity results show that the physics of the solution is self-consistent: as the  $S$ -wave speed of the cylinder tends to zero,

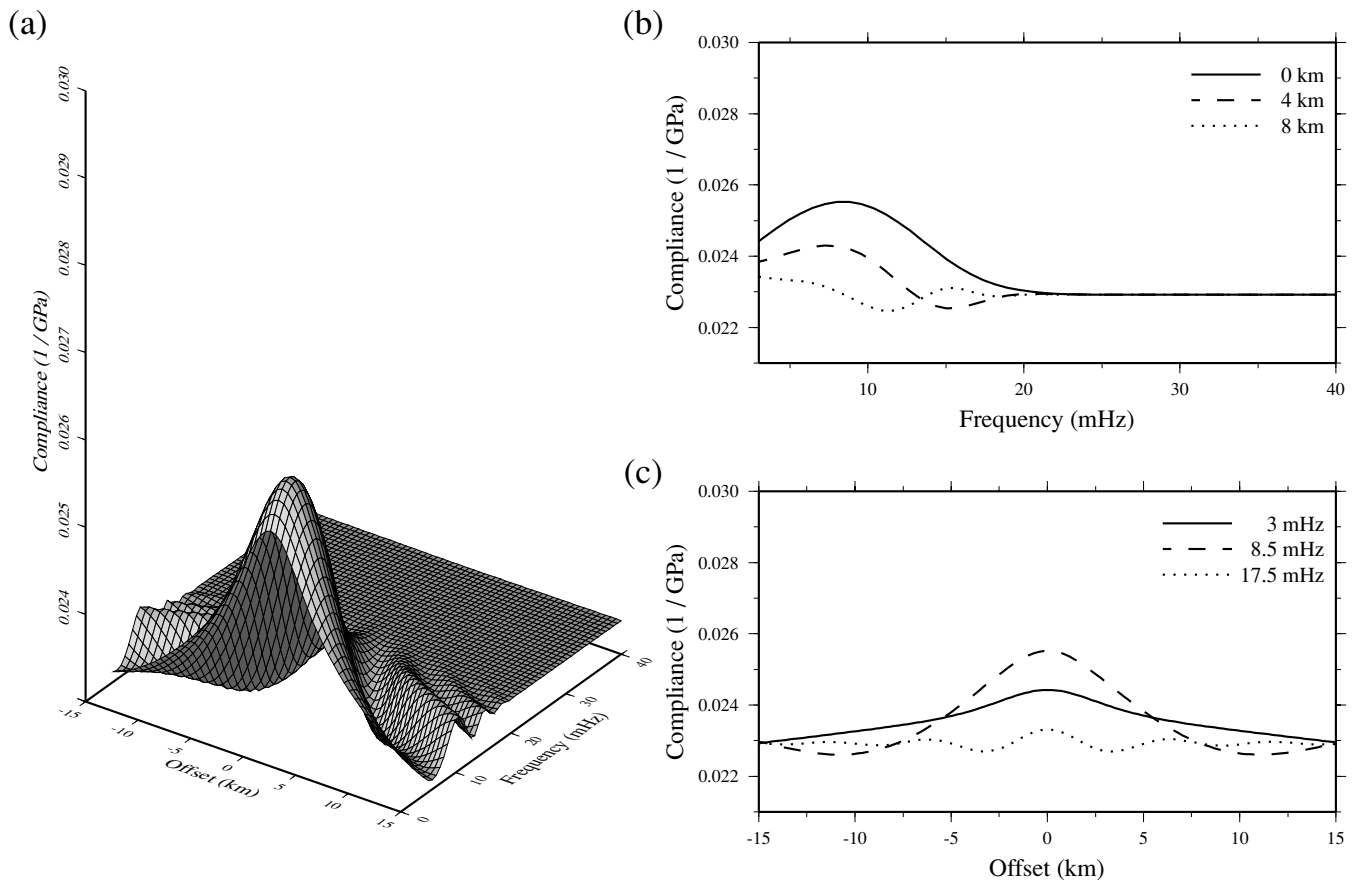


**Figure 6.** The amplitude of the compliance over a 1.2-km-radius mush cylinder placed at a depth of 5 km. (a) Compliance as a function of both frequency and offset. (b) Compliance as a function of frequency at selected offsets. (c) Compliance as a function of offset at selected frequencies.

the compliance response of an elastic cylinder tends towards the compliance response of a fluid cylinder.

Changing the  $S$ -wave speed of the background also principally affects the relative amplitude increase of the compliance peak, with increasing  $S$ -wave speed leading to larger relative amplitude increases. This increase is most pronounced for the medium shallow mush cylinder. As the background wave speed is varied, the compliance of the background will also change. From Fig. 8, a reduction in background  $S$ -wave speed increases both the value of the background compliance and the size (in absolute, but not relative terms) of the compliance peak caused by the cylinder.

The simplicity of our model means that we are restricted to a single wave speed throughout the entire background, whereas in reality the gross velocity structure around a mid-ocean ridge will show significant variation with depth. 1-D modelling indicates that any increase in background compliance at a given frequency will also increase the amplitude of the compliance signal from a low-velocity zone at the same frequency, even if the decrease in background velocity is at a different depth from the low-velocity zone. Surprisingly, this means in practical terms that a low-velocity zone within or below a low-velocity background should be more visible than a low-velocity zone in a high-velocity background.

### 3.2.2 Sensitivity to depth

Changing the depth of the cylinder affects all of the characteristic measurements of the compliance peak (Fig. 9). The relative amplitude increase of the compliance peak drops off rapidly as

the depth is increased, while the half-width of the spatial decay and the wavelength of the forcing that gives the peak response are both approximately proportional to the depth of the cylinder. The spatial half-width is approximately twice the depth to the centre of the cylinder and the peak wavelength is equal to approximately three times the depth. For 1-D problems it is found that the compliance is most sensitive to a forcing wavelength between 4 and 6 times the depth of a low-velocity feature (Crawford *et al.* 1998); the difference from the pattern of behaviour in the 1-D case is due to the lower frequency components sampling the stiffer structure to the sides of the cylinder and hence producing a smaller compliance response.

### 3.2.3 Sensitivity to radius

Fig. 9 also shows the sensitivity results for variations in the radius of the cylinder for the three models. Two sets of results are shown: in the first case the depth to the centre of the cylinder is kept fixed as the radius changes; in the second case the depth to the top of the cylinder is fixed, meaning that larger cylinders have their centres at greater depths.

The main effect in either case is on the amplitude of the compliance peak. With a fixed depth to the centre of the cylinder, the amplitude grows rapidly with increasing radius (approximately quadratically), whereas if the depth to the top of the cylinder is fixed, the growth rate is more or less linear with radius. For a given radius, and fixed depth to centre, the relative amplitude increase is greatest

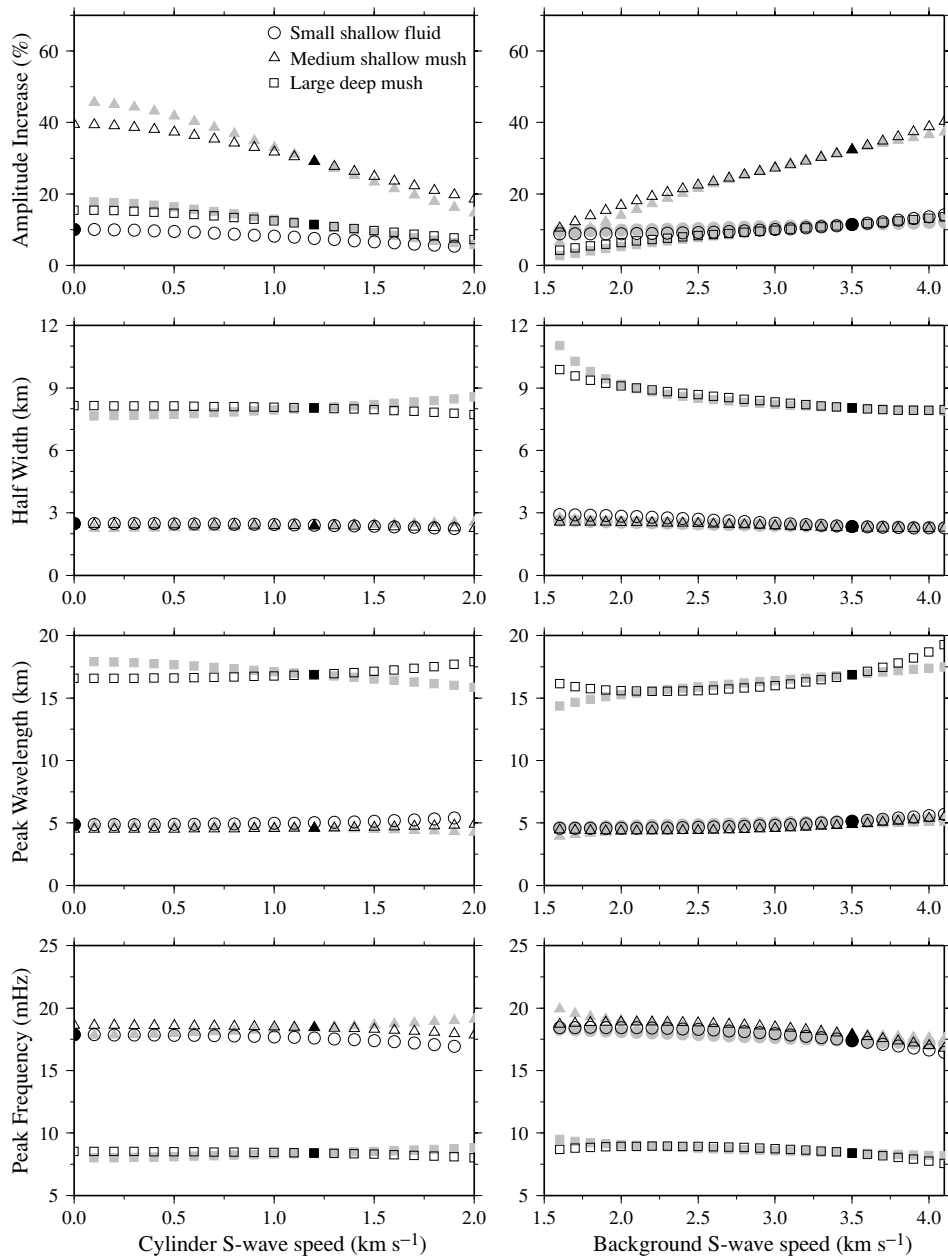


**Figure 7.** Sensitivity plots showing the variations in the relative amplitude increase of the peak compliance, the spatial half-width of the peak, and both the wavelength and corresponding frequency of the forcing that produces peak compliance signal as the *S*-wave velocities of the cylinder and the background are changed. Triangles correspond to the medium shallow mush cylinder of Fig. 3, circles to the small shallow fluid cylinder of Fig. 5, and squares to the large deep mush cylinder of Fig. 6. Values for the original models are indicated with solid black symbols. Solid grey symbols are for variation with a fixed Poisson ratio, hollow symbols are for variation with a fixed *P*-wave velocity.

for the fluid cylinder, consistent with the results for changing the *S*-wave speed of the cylinder shown in Fig. 7.

Surprisingly, the half-width of the compliance peak is not strongly affected by the radius of the cylinder. With a fixed depth to the centre of the cylinder, the half-width shows very little variation with radius, and even decreases slightly with increasing radius (probably caused by the shallowing of the cylinder's top). The results at very low values of the radius should not be considered too important because the very low amplitude of the response makes the measurements of Fig. 4 poorly defined. When the depth to the top of the cylinder is fixed, cylinders with larger radius produce greater half-widths, but the centres of these cylinders are at increasing depths,

and so it is not clear whether this pattern is primarily a width or a depth effect.

#### 4 1-D INVERSIONS

All previous experimental studies of compliance have used 1-D inversion of seafloor observed data to derive a *S*-wave structure of the crust (Crawford & Webb 2002). It is useful to test the validity of this approach for situations that show significant departures from a 1-D velocity structure. Applying a 1-D inversion to compliance calculated for a cylinder model allows us to investigate the limitation of this inversion technique for a model in which lateral variation is

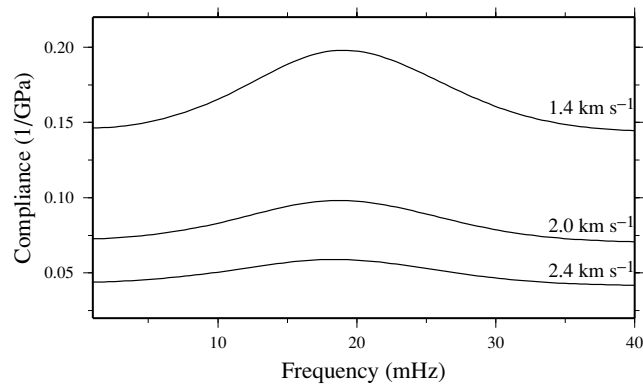


**Figure 8.** The effect of changing background  $S$ -wave speeds (marked on the plot) on the compliance peak generated by a fluid cylinder. The cylinder is of radius 600 m, with centre at 1.5 km depth. The  $P$ -wave speed of the cylinder is  $2.8 \text{ km s}^{-1}$  and the  $P$ -wave speed of the background is kept fixed at  $6 \text{ km s}^{-1}$ . Both cylinder and background have a density of  $2700 \text{ kg m}^{-3}$  and the water depth is 2.7 km.

important. Although it is simple, this model has the advantage of allowing accurate compliance calculations using the method of the previous section. Furthermore, we can use a relatively small number of parameters (wave speed, radius and depth of the cylinder) to assess the resolution of the resulting 1-D inversions.

#### 4.1 Test models and data

We carry out inversions of data from test models that consist of fluid cylinders of different radii with centres placed either at shallow or at deep depths beneath the seafloor (1.5 and 5 km, respectively). The shallow cylinders simulate a shallow melt lens whereas the deep cylinders represent melt near the crust–mantle boundary. The background medium has a  $P$ -wave speed of  $6.92 \text{ km s}^{-1}$ ,  $S$ -wave speed of  $3.76 \text{ km s}^{-1}$  and density  $2700 \text{ kg m}^{-3}$ . The  $P$ -wave speed in the shallow cylinder is  $2.61 \text{ km s}^{-1}$  and its density is  $2700 \text{ kg m}^{-3}$ . The  $S$ -wave speed is zero, representing a pure melt lens. The compliance data that is used in the inversions is calculated using the method described earlier, and we consider inversions of data corresponding to instrument locations both directly over the centre of the cylinder and offset a certain distance to the side.

We perform minimum structure 1-D inversions for  $S$ -wave velocity structure using a starting model of a uniform half-space with material parameters equal to those of the background model. The inversion seeks the smoothest model that fits the data to within a prescribed error range, and thus the inversion result can be heavily dependent on the size of the error assigned to the data. The errors that we use are calculated using the method of Crawford *et al.* (1991), using values of pressure and noise derived from actual compliance measurements. We take the pressure spectrum to be flat within the compliance band with a power spectral density of  $10^4 \text{ Pa}^2 \text{ Hz}^{-1}$ , which is at the lower end of values measured in the Pacific Ocean (Webb *et al.* 1991; Crawford 2004). In a real experiment, data are stacked using 20-min windows to increase the signal-to-noise ratio (e.g. Crawford & Webb 2002). We assume that the compliance instrument is placed on the seafloor for either a 2-day interval (the ‘standard error’ case, equivalent to 100 event-free data windows) or a 2-week interval (1000 data windows; the same errors would be obtained for a 2-day deployment if the pressure spectrum was 10 times as powerful). The 2-day deployment time corresponds to a normal experiment whereas a 2-week deployment could be used

to improve resolution and leave a significant amount of ship time available for a co-joint active seismic program.

The 1-D forward modelling is carried out using a reflectivity method (Gomberg & Masters 1988; Crawford *et al.* 1991), and the iterative inversion is performed in the wavenumber domain using a linear approximation in a least squared sense. The misfit between the data (obtained analytically for the cylinder) and the synthetic (reflectivity response) is minimized using a steepest descent method. The inversion holds the  $P$ -wave speed and the density constant and only inverts for  $S$ -wave structure. The velocity model is parametrised as a stack of 34 layers, increasing in thickness from 50 m at the seafloor by a factor of 1.1 for each subsequent layer, with a half-space assumed below a depth of 11 km.

The minimum structure inversion will recover the smoothest possible velocity structure that fits the data to within the prescribed error tolerance. This method explicitly penalises high gradients in the velocity model, and so we do not expect it to recover the true velocity structure in this instance. Instead, this type of inversion is most useful as a tool to see if the presence of low-velocity zones is required by the data. In practice, compliance data is unlikely to be the only source of geophysical information. The inclusion of seismic reflection or refraction data as *a priori* information in a Bayesian inversion, or directly in a joint seismic and compliance inversion, allows much tighter constraints on the velocity structure of the crust (Hulme *et al.* 2003).

#### 4.2 Shallow melt lens

We firstly consider the ability of a 1-D inversion to recover evidence of a shallow melt lens, of the type found along large parts of the East Pacific Rise. We begin by investigating the role of the error level on the inversion results. Fig. 10 shows the effect of deployment length on errors and inversion sensitivity, using a 400-m-radius fluid cylinder with centre at 1.5 km depth. For errors corresponding to a 2-day deployment the inversion simply puts low velocities in the upper 2-km of the seafloor. As the deployment length is increased, and so the error decreased, the inversion recovers the low-velocity anomaly at an appropriate depth but the anomaly is smeared out over a large depth range. The smearing is more pronounced below the cylinder than at the top of it. This better resolution of the top of the cylinder is expected, as the depth sampled by the compliance data depends on the forcing wavelength, and so deeper structure is sampled by longer wavelength waves. The velocity contrast of the anomaly is poorly recovered, which, as discussed above, is characteristic of a minimum structure inversion.

Our next objective is to test the size of cylindrical anomaly that could be successfully recovered using 1-D inversion when the instrument is placed directly above the cylinder. Results for cylinders with radius from 300–800 m and centre at 1.5 km depth are shown in Fig. 11. We find that with the standard error level corresponding to the 2-day deployment, the inversion can recover distinct low-velocity zones for cylinders with radius 500 m or greater. With an error level corresponding to the longer deployment, cylinders down to 300 m radius are detected. For the 400-m-radius cylinder using the standard error level, a low-velocity structure is recovered near the seafloor but no clear low-velocity anomaly is observed; when the lower error level is used the anomaly is very well recovered (Figs 10b and 11). The amplitude of the recovered velocity anomaly increases with the increasing radius of the cylinders (Fig. 11), and the 800 m radius cylinder is very well recovered with error levels corresponding to either deployment length. The centre of the anomaly is somewhat shallower than the centre of the cylinder, which may be due to the

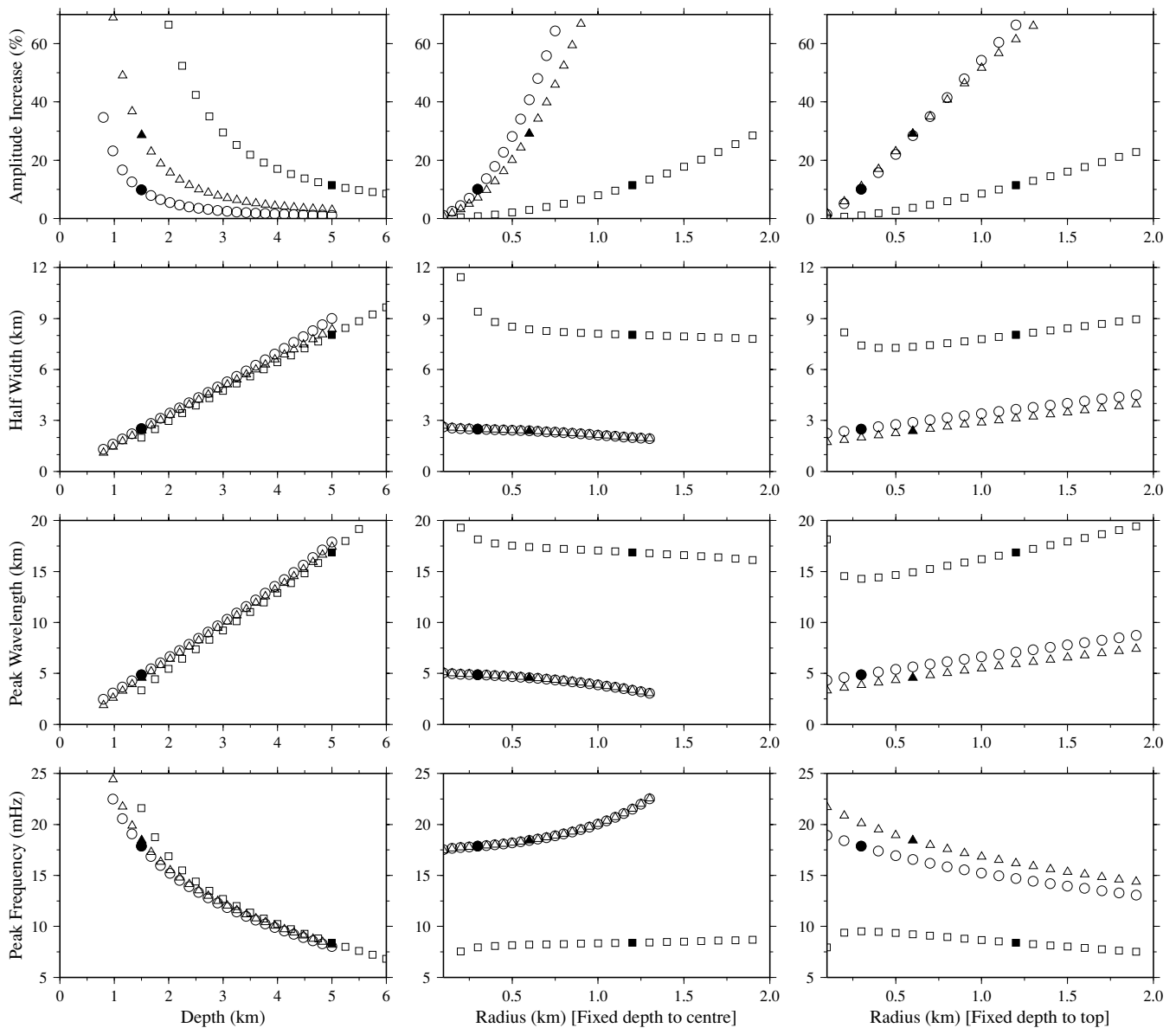


**Figure 9.** Sensitivity plots as in Fig. 7, but for variations in cylinder depth and in cylinder radius (keeping either the depth to the centre of the cylinder or the depth to the top of the cylinder fixed).

different depth sensitivity of compliance to 1-D and 2-D structures, as discussed above. Even the lowest velocity recovered ( $2.4 \text{ km s}^{-1}$  for the short deployment,  $2.3 \text{ km s}^{-1}$  for the longer deployment) is much higher than the  $0 \text{ km s}^{-1}$  in the original model. The recovered velocities near the seafloor are lower than the background velocity, due to both the nature of the minimum structure inversion and the finite resolution of the compliance method.

As well as inverting data recorded directly over the centre of the cylinder, we can also consider inversions of data from locations offset to the side. As was shown above (e.g. Fig. 3b), the peak amplitude of the seafloor compliance decreases away from the centre of the cylinder, and the peak frequency also decreases, suggesting that with increasing distance from the cylinder the 1-D inversions will place smaller lower velocity zones deeper in the seafloor. Fig. 12 shows inversions for a 600-m-radius shallow fluid cylinder (1.5 km depth), at offsets up to 7.5 km. The strongest anomaly is recovered at zero offset, and it is centred at slightly shallower than the correct depth. At 2.5 km offset, slightly less than twice the depth of the

cylinder, the anomaly is still recovered but the anomaly amplitude is much smaller. The velocity above and below the cylinder is higher than the background velocity, which is due to both the oscillatory nature of the seafloor data from the cylinder and to the resistance of the minimum structure inversion to rapid changes in model gradient. The peak of the anomaly is slightly deeper than the depth of cylinder, which could be due to shift of peak amplitude towards the lower frequencies. With the decreased error level corresponding to a longer deployment, the anomaly is more pronounced, as are the oscillations. Beyond 5 km offset, no low-velocity anomalies are observed with the levels of error corresponding to the standard deployment length, providing the maximum offset limit where the anomaly could be recovered (2.5–5 km).

### 4.3 Deep melt anomaly

To test the effect of a deep melt body, seafloor compliance data was computed for a fluid cylinder of 1 km radius placed at 5 km below

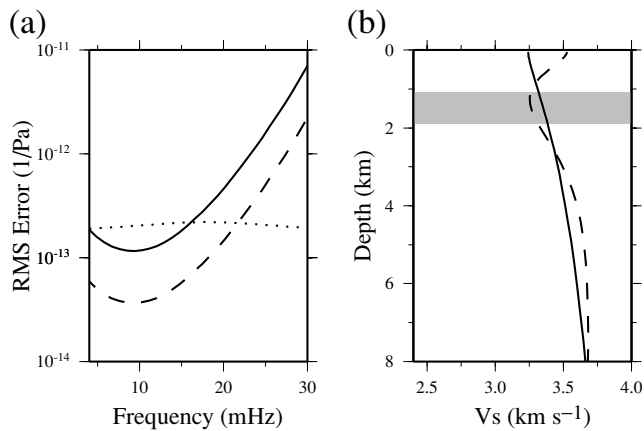


**Figure 10.** The effect of the rms error values on a 1-D inversion, for a fluid cylinder with radius 400 m with centre at 1.5 km depth. (a) Solid line: errors characteristic of a 2-day deployment; dashed line: errors characteristic of a 2-week deployment. For reference, errors equal to 1 per cent of the compliance value are shown by the dotted line. (b) The inverted velocity structures. The grey box shows the location of the cylinder in the original model.

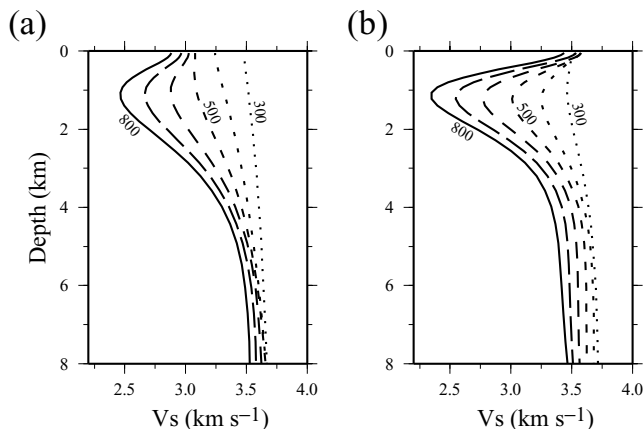


**Figure 11.** Inversions for a shallow melt lens with cylinder radii (from right to left) of 300 m, 400 m, 500 m, 600 m, 700 m and 800 m. (a) Standard levels of error, corresponding to a 2-day deployment. (b) Reduced error levels, corresponding to a 2-week deployment.

the seafloor, simulating a melt body just above the Moho. The larger diameter was necessary to obtain a value for the compliance signal that stood out from the error level. Fig. 13 shows inversions of these calculations, again for a range of offsets. For the zero offset case, the inverted velocity decreases linearly from about  $3.6 \text{ km s}^{-1}$  at the seafloor to about  $3.1 \text{ km s}^{-1}$  at 5 km depth and remains more or less constant down to 8 km depth. At an offset of 2.5 km, the inverted velocity structure shows similar features to that at zero offset but the velocity is about  $250 \text{ m s}^{-1}$  higher at all depths. The near surface velocities recovered by the inversion are slightly lower than the background velocity for offsets of 5 km and 7.5 km. At 5 km offset, the inverted velocity is highest at 2 km depth and then smoothly decreases to  $2.9 \text{ km s}^{-1}$  at 8 km depth. The result for the offset of 7.5 km is similar, but the peak is deeper (4 km) and the velocity decreases to  $2.95 \text{ km s}^{-1}$  at 8 km depth. In addition, with lower error levels (corresponding to a longer deployment time), a second low-velocity zone is recovered at 1.5 km depth. The presence of this zone in the inversion is caused by secondary peaks seen in off-axis compliance data due to Rayleigh wave modes, which are

unimportant over the body but may dominate at the flanks. This artefact demonstrates the importance of having measurements at multiple locations to put lateral effects in context. Using the lower error levels does not lead to any great improvement in the resolution of the inversions. The 1-D inversions are able to identify the presence of low-velocity anomaly at the Moho depth but its size and amplitude are difficult to resolve.

## 5 DISCUSSION AND CONCLUSIONS

The sensitivity tests have allowed us to investigate the major controls on the compliance over a cylindrical object. The compliance for this 2-D model shows a similar sensitivity to low  $S$ -wave speeds as for 1-D models, exhibiting a strong peak over the location of the low-velocity zone. Although the amplitude of the peak increases as the cylinder's  $S$ -wave speed drops, it is difficult to distinguish between regions that are pure liquid and those that have a low (but non-zero)  $S$ -wave speed. The amplitude of the compliance peak also depends strongly on the depth and the radius of the anomaly: shallower depths and larger radii give greater peak amplitudes. Both the wavelength of the forcing generating the peak compliance and the spatial half-width of the peak depend mainly on the depth to the cylinder. The heuristic evidence of the sensitivity tests is therefore that compliance data should be able to place quite strong constraints on the depth to a low-velocity zone, but there may be a trade-off between the size of the anomaly and its  $S$ -wave speed.

The 1-D inversions of 2-D data have allowed us to investigate what structure can be recovered using this method of inversion. Because this inversion is highly non-linear, it is not straightforward to predict what features will be robustly constrained. During our modelling and inversion of shallow anomalies, we placed different-sized cylinders with centres at 1.5 km depth. The effect of changing the size of the cylinder is compounded by the effect that the smaller the radius, the deeper the top of the cylinder will be. A 1-D inversion was able to recover a low-velocity anomaly over a fluid cylinder of 600 m radius, under normal levels of measurement error. For a higher signal to noise ratio corresponding to a longer instrument deployment time or higher ocean pressure levels, it became possible to recover the depth of a cylinder of 300 m radius. As expected, the imaged results are smeared over a greater depth range, and the top of the cylinder is better recovered than the bottom of the cylinder. For a shallow cylinder, it is not possible to recover the anomaly at offsets significantly more than twice the depth. This offset is approximately equal to the half width of the anomaly (Fig. 9). These results suggest that we should place seafloor compliance instruments at least a half-width interval. They also suggest that if similar anomalies are observed at far distances from each other, they are caused by local structure (Crawford & Webb 2002). For a shallow low-velocity zone at 1.5 km depth, the half-width is approximately 3 km. Compliance measurements made with this spacing will ensure that any shallow low-velocity zones found in the inversion are indeed due to shallow structure, and not caused by the secondary peaks of the compliance over a deep crustal feature.

Crawford *et al.* (1999) used compliance data collected across the East Pacific Rise axis at  $9^{\circ}48'N$  to model a several-kilometre-wide region of partial melt (with an average  $S$ -wave speed of  $1.7 \text{ km s}^{-1}$ ) in the lower crust overlying a narrow near-Moho melt body (less than 1 km wide, with  $S$ -wave speed less than  $0.05 \text{ km s}^{-1}$ ). Because their 2-D finite-difference scheme could not model a small pure melt body, they calculated the compliance of the Moho melt body by laterally filtering compliance values from 1-D models

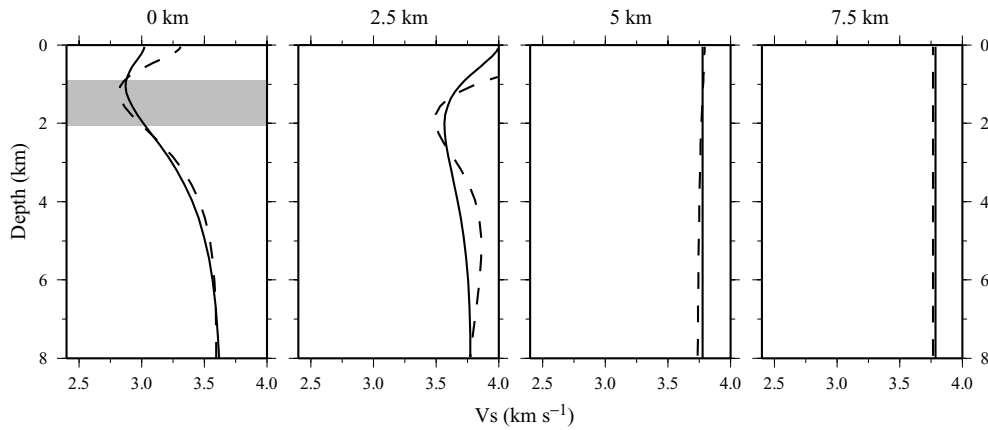


**Figure 12.** Inversions of compliance data from different offsets for a 1.5 km deep, 600-m-radius cylinder. Solid line: errors characteristic of a 2-day deployment; dashed line: errors characteristic of a 2-week deployment. The grey box in the inversion for zero offset shows the location of the cylinder in the original model.

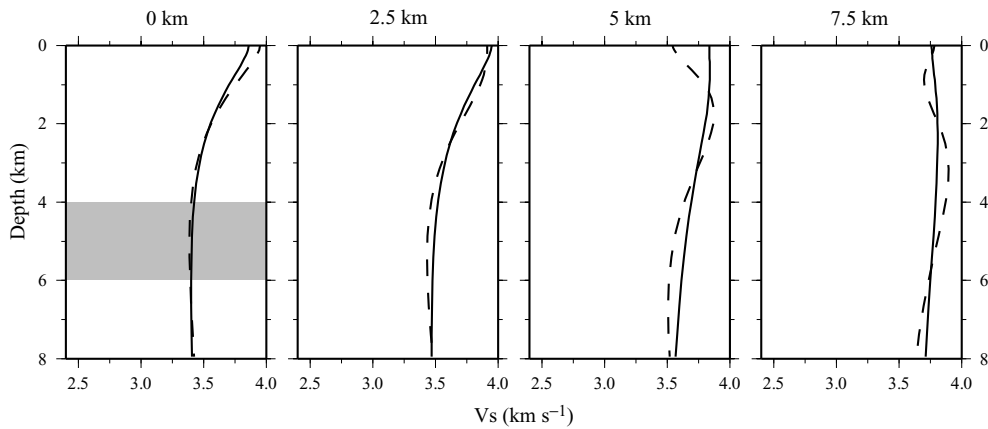


**Figure 13.** Inversion of compliance data from different offsets from a 5 km deep, 1000-m-radius cylinder. Solid line: errors characteristic of a 2-day deployment; dashed line: errors characteristic of a 2-week deployment. The grey box in the inversion for zero offset shows the location of the cylinder in the original model.

(Crawford *et al.* 1991). Their low velocity estimate for the near-Moho body is based on the nearly exponential increase in 1-D compliance as the  $S$ -wave speed approaches zero. The 2-D modelling in this paper indicates that the compliance peak over such a narrow body will not increase exponentially in this way, suggesting that that the body could have a significantly higher  $S$ -wave speed than they estimated (the peak in compliance is about the same for objects with an  $S$ -wave speed in the range 0–0.5 km s<sup>-1</sup>), and that the body must be much larger than they estimated. Unfortunately, we can not directly use the results of this paper to estimate the size of the deep low velocity body observed by Crawford *et al.* (1999) at the EPR because an accurate fit to the compliance data requires a non-uniform background velocity and perhaps a different shape to any inferred melt body.

Most melt bodies at mid-ocean ridges are believed to be much wider than tall, and it is reasonable to speculate that they may generate a compliance behaviour somewhere between that of the 1-D and cylindrical cases. 1-D models with low-velocity layers produce much larger compliance responses than do cylinders of the same thickness (compare Figs 1 and 3: the low-velocity layer is 400 m thick while the cylinder has a radius of 600 m), and so it may be the case that a thin, wide melt body gives a compliance signal much larger than that of a cylinder with the same volume.

The detailed modelling of the compliance behaviour of such bodies remains a challenge, however, since their thickness will often be

below the resolution that can currently be obtained in a reasonable time using a finite-difference code. Extending the analytical solution presented in this paper to other shapes (e.g. ellipses) presents significant theoretical difficulty, since the solutions to the Helmholtz equation found by separation of variables in other coordinate systems are less amenable to analysis. It may, however, be possible to efficiently model the compliance response of isolated bodies of arbitrary shape using a boundary integral method to represent the scattered wavefield—the method is analogous to that presented here in that the scattered wavefield is represented as a sum of point source solutions to the wave equation. The weights of each point source solution are found numerically by solving equations imposing continuity of displacement and traction at the boundary of the scattering body (e.g. Benites *et al.* 1997). The best way to model different, more complicated geometries (including those with non-uniform background velocities) may be by using finite elements. Finite-element modelling is likely to be at least as slow as finite differences, and therefore unusable for data inversions. However, we could use this method to investigate the effect of more complicated melt body shapes and variable background velocity structures, and to check inversion results obtained using simpler approximations such as the pseudo-2-D method outlined in Crawford *et al.* (1998).

In this paper we have considered compliance data in isolation. In practice, other geophysical techniques, such as seismic

reflection or refraction data, are able to provide much *a priori* data about low-velocity anomalies. Integrating this information into the compliance inversion should give much tighter constraints on the velocity structure of the subsurface.

1-D inversion is likely to remain for some time the most common method used to analyse seafloor compliance data, as any other currently available modelling scheme is computationally too intensive for use in an inversion scheme. The results of this paper show that, despite the clear shortcomings of a 1-D assumption within the context of a mid-ocean ridge environment, a 1-D inversion is able to identify and to locate shallow low-velocity zones, and is also able to indicate regions of low velocity within the lower crust. These results illustrate the potential of seafloor compliance, particularly when used in conjunction with other complementary geophysical techniques, to provide valuable information about the structure of the oceanic crust.

## ACKNOWLEDGMENTS

We are grateful for the helpful comments of editor Gabi Laske, and careful reviews from Harm Van Avendonk and an anonymous reviewer.

## REFERENCES

- Acheson, D.J., 1990. *Elementary Fluid Dynamics*, Oxford University Press, Oxford.
- Benites, R.A., Roberts, P.M., Yomogida, K. & Fehler, M., 1997. Scattering of elastic waves in 2-D composite media I. Theory and test, *Phys. Earth planet. Int.*, **104**, 161–173.
- Crawford, W.C., 2004. The sensitivity of seafloor compliance measurements to sub-basalt sediments, *Geophys. J. Int.*, **157**, 1130–1145.
- Crawford, W.C. & Webb, S.C., 2002. Variations in the distribution of magma in the lower crust and at the Moho beneath the East Pacific Rise at 9–10°N, *Earth planet. Sci. Lett.*, **203**, 117–130.
- Crawford, W.C., Webb, S.C. & Hildebrand, J.A., 1991. Seafloor compliance observed by long-period pressure and displacement measurements, *J. geophys. Res.*, **96**, 16 151–16 160.
- Crawford, W.C., Webb, S.C. & Hildebrand, J.A., 1998. Estimating shear velocities in the oceanic crust from compliance measurements by two-dimensional finite difference modeling, *J. geophys. Res.*, **103**, 9895–9916.
- Crawford, W.C., Webb, S.C. & Hildebrand, J.A., 1999. Constraints on melt in the lower crust and Moho at the East Pacific Rise, 9°48'N, using seafloor compliance measurements, *J. geophys. Res.*, **104**, 2923–2939.
- Gomberg, J.S. & Masters, T.G., 1988. Waveform modeling using locked-mode synthetic and differential seismograms: application to determination of the structure of Mexico, *Geophys. J.*, **94**, 193–218.
- Hulme, T., Ricolleau, A., Bazin, S., Crawford, W.C. & Singh, S.C., 2003. Shear wave structure from joint analysis of seismic and seafloor compliance data, *Geophys. J. Int.*, **155**, 514–520.
- Jeffreys, H. & Jeffreys, B.S., 1956. *Methods of Mathematical Physics*, 3rd edn, Cambridge University Press, Cambridge.
- Kelemen, P.B. & Aharonov, E., 1998. Periodic formation of magma fractures and generation of layered gabbros in the lower crust beneath oceanic spreading ridges, in *Faulting and Magmatism at Mid-ocean Ridges*, eds Buck, W.R., Delaney, P.T., Karson, J.A. & Lagabriele, Y., American Geophysical Union, Washington, DC.
- Latychev, K. & Edwards, R.N., 2003. On the compliance method and the assessment of three-dimensional seafloor gas hydrate deposits, *Geophys. J. Int.*, **155**, 923–952.
- Liu, Y., Wu, R.-S. & Ying, C.F., 2000. Scattering of elastic waves by an elastic or viscoelastic cylinder, *Geophys. J. Int.*, **142**, 439–460.
- MacLennan, J., Hulme, T. & Singh, S.C., 2005. Cooling of the lower oceanic crust, *Geology*, **33**, 357–360, doi:10.1130/G21207.1.
- Pao, Y.H. & Mow, C.C., 1973. *Diffraction of Elastic Waves and Dynamic Stress Concentrations*, Crane Russak, New York.
- Singh, S.C., Kent, G.M., Collier, J.S., Harding, A.J. & Orcutt, J.A., 1998. Melt to mush variations in crustal magma properties along the ridge crest at the southern East Pacific Rise, *Nature*, **394**, 874–878.
- Webb, S., Zhang, X. & Crawford, W.C., 1991. Infragravity waves in the deep ocean, *J. geophys. Res.*, **96**, 2723–2736.